UXO DISCRIMINATION USING TIME DOMAIN ELECTROMAGNETIC INDUCTION

Leonard R. Pasion, Stephen D. Billings, and Douglas W. Oldenburg
UBC - Geophysical Inversion Facility
Department of Earth and Ocean Sciences, University of British Columbia
Vancouver, B.C., V6T 1Z4, CANADA
email: pasion@geop.ubc.ca

Category: **Detection**

1 Introduction

An explosive ordnance is a munition that is either launched or fired with the intent of detonation at a specified target. An unexploded ordnance (UXO) is an explosive ordnance that, due to some malfunction, remains undetonated. As a result, the ordnance can be found at the ground surface, partially buried, or buried at a depth of up to 8 m beneath the surface. Practical and cost-effective strategies for remediation require both detection of possible targets and the ability to discriminate between UXO and contaminating scrap metal.

The detection of buried metallic objects can be accomplished with a variety of geophysical sensing techniques. Time domain electromagnetic induction (TEM) surveys have been successful in detecting both ferrous and non-ferrous metallic objects near the soil surface, and are a mainstay amongst technologies currently utilized in UXO clearance projects. In the TEM method a time varying magnetic field is used to illuminate a conducting target. This primary field induces surface currents on the target which then generate a secondary magnetic field that can be sensed above ground. As time elapses, the surface currents diffuse inwards, and the observed secondary field consequently decays. The rate of decay, and the spatial behavior of the secondary field, is determined by the target's conductivity, magnetic permeability, shape, and size.

In Pasion and Oldenburg (2000) we presented a TEM data inversion algorithm for estimating the basic shape (rod-like or plate-like) and magnetic character (ferrous or non-ferrous) of a buried metallic object. In this report, after briefly outlining the inversion algorithm, we apply the algorithm to two field examples. In the first example a Geonics EM63 survey was carried out over a $2m \times 2m$ area over a 60 mm mortar. For the second example TEM data were collected over a seeded UXO test site at the former Fort Ord in California. An $8ft \times 8ft$ portion of the data, centered over one of the anomalies, was extracted from the data set.

2 Development of Approximate Forward Modelling

In order to invert measured TEM data for the physical parameters of the target, it is necessary to have a forward model to describe the TEM response for a buried metallic object. We can restrict our forward model to axi-symmetric metallic targets, since this geometric subset adequately describes all UXO and the majority of buried metallic scrap encountered in a remediation survey. Unfortunately, analytic expressions for the time domain response are restricted to a metallic sphere, and even an expression for a permeable and conducting non-spherical axi-symmetric body is not available. Numerical solutions of Maxwell's equations, under continual development, are promising (e.g. Haber, 2000; Carin, 2000; Hiptmair, 1998), however, the computational time requirements for obtaining a solution still make them impractical for use as part of a rigorous inversion procedure. Our approach, therefore, is to use an approximate forward model that can adequately reproduce the measured electromagnetic anomaly with minimal computational effort. The validity of this reduced modelling still needs further testing but the empirical tests carried out here (and in Pasion and Oldenburg (2000)) suggest that it can be useful in practice.

Our approximate forward modelling represents the time domain response of a metallic object as a pair of perpendicular dipoles located at the center of the buried target. The modelled reponse can either be measurements of the secondary magnetic field ($\mathbf{B}$-field), or the derivative of the secondary magnetic field ($\partial\mathbf{B}/\partial t$). We consider a target whose center is located at $\mathbf{R} = (X, Y, Z)$ in the space-fixed co-ordinate system (fig. 1).

The secondary response $\boldsymbol{\xi}(\mathbf{r}, t)$, representing either $\mathbf{B}$-field or $\partial\mathbf{B}/\partial t$ data, measured at a receiver/transmitter location $\mathbf{r}$ and at a time t after the termination of the primary field, is then the sum of the responses of the two orthogonal dipoles:

$$\boldsymbol{\xi}(\mathbf{r}, t) = \boldsymbol{\xi}_1(\mathbf{r}, t) + \boldsymbol{\xi}_2(\mathbf{r}, t) \tag{1}$$

where

$$\boldsymbol{\xi}_i(\mathbf{r}, t) = \frac{\mu_o}{4\pi}\left(3\left[\mathbf{m}_i(t)\cdot(\mathbf{r}-\mathbf{R})\right]\frac{(\mathbf{r}-\mathbf{R})}{|\mathbf{r}-\mathbf{R}|^5} - \frac{\mathbf{m}_i(t)}{|\mathbf{r}-\mathbf{R}|^3}\right) \tag{2}$$

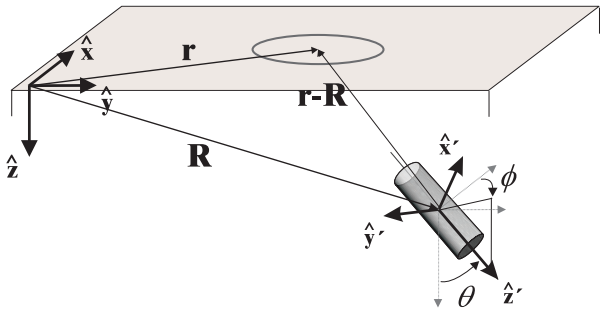

Figure 1: The field co-ordinate system for a buried target.

and

$$\mathbf{m}_1(t) = L_1(t)\,(\hat{\mathbf{z}}' \cdot \mathbf{B}^p)\,\hat{\mathbf{z}}' \tag{3}$$

$$\mathbf{m}_2(t) = L_2(t)\left[(\hat{\mathbf{x}}' \cdot \mathbf{B}^{\mathbf{P}})\,\hat{\mathbf{x}}' + (\hat{\mathbf{y}}' \cdot \mathbf{B}^{\mathbf{P}})\,\hat{\mathbf{y}}'\right] \tag{4}$$

are the dipole parallel and perpendicular to the axis of symmetry. The unit vectors $\hat{\mathbf{x}}'$, $\hat{\mathbf{y}}'$, and $\hat{\mathbf{z}}'$ are given by

$$\hat{\mathbf{x}}' = \cos\phi\cos\theta\,\hat{\mathbf{x}} + \sin\phi\cos\theta\,\hat{\mathbf{y}} - \sin\theta\,\hat{\mathbf{z}} \tag{5}$$

$$\hat{\mathbf{y}}' = -\sin\phi\,\hat{\mathbf{x}} + \cos\phi\,\hat{\mathbf{y}} \tag{6}$$

$$\hat{\mathbf{z}}' = \cos\phi\sin\theta\,\hat{\mathbf{x}} + \sin\phi\sin\theta\,\hat{\mathbf{y}} + \cos\theta\,\hat{\mathbf{z}}. \tag{7}$$

$L_1(t)$ and $L_2(t)$ characterize the time decay behaviour of the the two dipoles. An appropriate form for the decay law of either $\mathbf{B}$-field or $\partial\mathbf{B}/\partial t$ data is

$$L_i(t) = k_i\,(t+\alpha_i)^{-\beta_i}\,e^{-t/\gamma_i}. \tag{8}$$

The validity of this decay law was established in Pasion (1999).

In summary, the approximate response of buried metallic object given by eq. (1) can be generated from 13 parameters that describe the object. These model parameters are elements of the model vector

$$\mathsf{m} = [X,\, Y,\, Z,\, \phi,\, \theta,\, k_1,\, \alpha_1,\, \beta_1,\, \gamma_1, k_2,\, \alpha_2,\, \beta_2,\, \gamma_2]\,. \tag{9}$$

X and Y denotes the surface projection of the centroid of the body, and Z is the depth of the object below the surface. The orientation of the target is described by the two angles θ and ϕ. The remaining parameters describe the decay characteristics of the two dipoles: k_1, α_1, β_1, and γ_1 describe the dipole parallel to the axis of symmetry ($\mathbf{m}_1$), and k_2, α_2, β_2, and γ_2 describe the dipole perpendicular to the axis of symmetry ($\mathbf{m}_2$). Thus the inversion for the model m will immediately give estimates of target location and orientation. Information on the shape, size, and material parameters of the target may later be inferred from the remaining parameters.

3 Non-Linear Parameter Estimation Procedure

In this paper it is assumed that the response measured in a survey is due to a single body, and second, that the response of this single body can be accurately modelled with eq. (1). With these assumptions, an inversion procedure can be developed that utilizes the approximate forward model.

The forward model can be expressed as

$$d_j = F_j[\mathsf{m}], \qquad j = 1, 2, 3, \ldots N \tag{10}$$

This equation expresses the mapping of the model vector m to a datum d_j by a functional F_j. The forward mapping F_j is defined by eq. (1) and it is a nonlinear functional of the 13 model parameters given in eq. (9). In the inverse problem, these parameters are retrieved from a vector of observed data d^{obs} by minimizing a least-squares objective function:

$$\Phi(\mathsf{m}) = \frac{1}{2}\|\mathsf{W}_d\left(F[\mathsf{m}] - \mathsf{d}^{obs}\right)\|^2 \tag{11}$$

where $F[\mathsf{m}]$ is the forward modelled data, d^{obs} is the observed data, and Φ is the least squares objective function that measures how closely our predicted data matches the observed data. W_d is the data weighting matrix. If the data are contaminated with unbiased Gaussian random noise, then W_d is ideally a diagonal matrix whose elements are the reciprocals of the standard deviation of each datum.

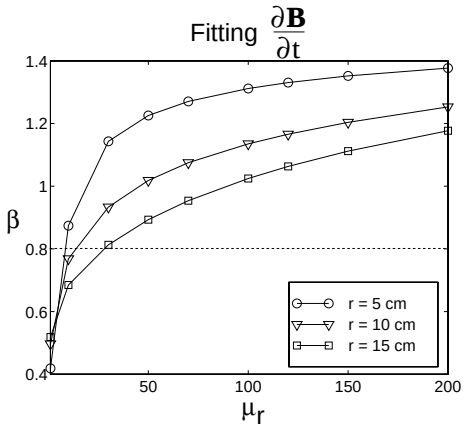

Figure 2: The behaviour of parameter β for various size spheres with varying permeability μ.

4 Relating Model Parameters to Material and Geometric Properties

The above inversion procedure is used to recover parameters that characterize a target's TEM anomaly. The next step is to interpret these parameters. Recall that UXO are typically rod-like rather than plate-like, and are magnetically permeable. In order to extract these potentially UXO identifying features from the recovered model vector (eq. (9)), we use the inversion procedure to fit a series of decay curves from a range of axi-symmetric targets of different shape, geometry, and material properties. We then generate empirical relationships between the parameters and target characteristics. The data curves used for this analysis were either TEM measurements made in the Geonics Ltd. laboratory, or they were synthetically generated decay curves for a sphere using equation (1).

In this paper we present the analysis of the $\partial\mathbf{B}/\partial t$ response of the targets, and refer the reader to Pasion (1999) for the analysis of the $\mathbf{B}$-field data. There we show that the same target shape diagnostics, developed here for $\partial\mathbf{B}/\partial t$ data, also apply to $\mathbf{B}$-field data.

4.1 A Relationship Between β and Magnetic Permeability

UXO are generally made of steel, which is a ferrous material. Therefore, the magnetic permeability is likely an identifying characteristic of UXO. To generate a link between magnetic permeability and model parameters, forward modelled responses were calculated for a series of spheres varying in size and permeability. $\partial\mathbf{B}/\partial t$ data were then inverted to generate decay parameters, and in particular, to produce estimates of the parameter β. The plots of β as a function of sphere radii and magnetic permeability, are provided in fig. 2. Fig. 2 suggests that when applying our inversion to the time derivative of the field, a value of β greater than about 0.8 indicates that the target is most likely permeable. The use of β as a diagnostic to determine permeability can be extended to non-spherical targets by looking at the recovered β values for the aluminum and steel prisms. The inversion produces two values of β, one for each of the excited dipoles, to describe a buried target. We suggest taking the average of the two recovered β values, which we label as $\bar{\beta}$.

4.2 Relationships Between Model Parameter Ratios and Target Shape

The Ratio k_1/k_2. The recovered k-ratio for targets ranging from a steel plate to a steel rod are shown in fig. 3(a). For a steel plate, the k-ratio $k_1/k_2 < 1$, while for a steel bar the k-ratio $k_1/k_2 > 1$. The opposite orientation effect was observed for an aluminum rod, that is $k_1/k_2 < 1$ (fig. 3(b)).

The Ratio β_1/β_2. The recovered β-ratio for targets ranging from a steel plate to a steel rod are shown in fig. 4(a). For a steel plate, the β-ratio $\beta_1/\beta_2 > 1$, while for a steel bar the β-ratio $\beta_1/\beta_2 < 1$. The decay curves for aluminum targets are essentially the same regardless of target shape, and therefore there is no relationship between the β-ratio and the aspect ratio (fig. 4(b)).

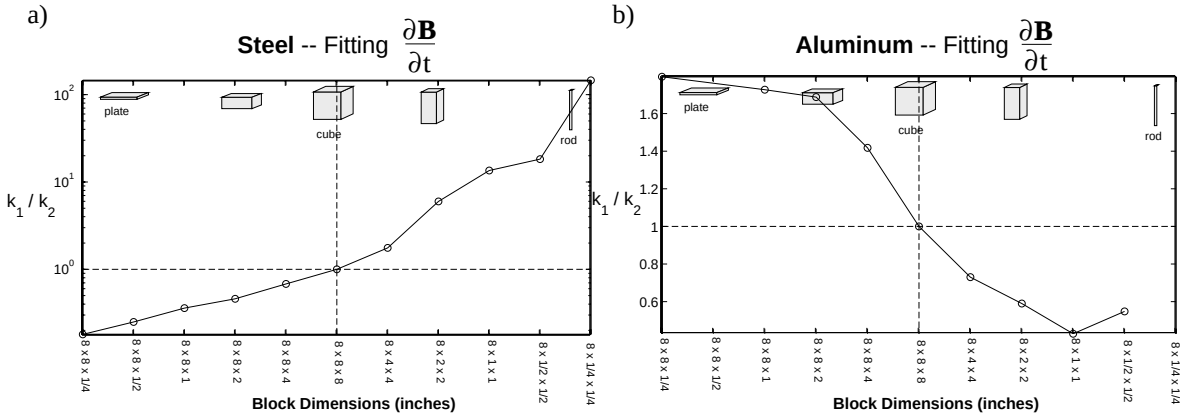

Figure 3: Relating the aspect ratio of a steel target with the ratio k_1/k_2. Plot (a) illustrates the relationship between the k_1/k_2 ratio derived from $\partial\mathbf{B}/\partial t$ data and the shape of a steel target. Plot (b) illustrates the relationship between the k_1/k_2 ratio and the shape of an aluminum target.

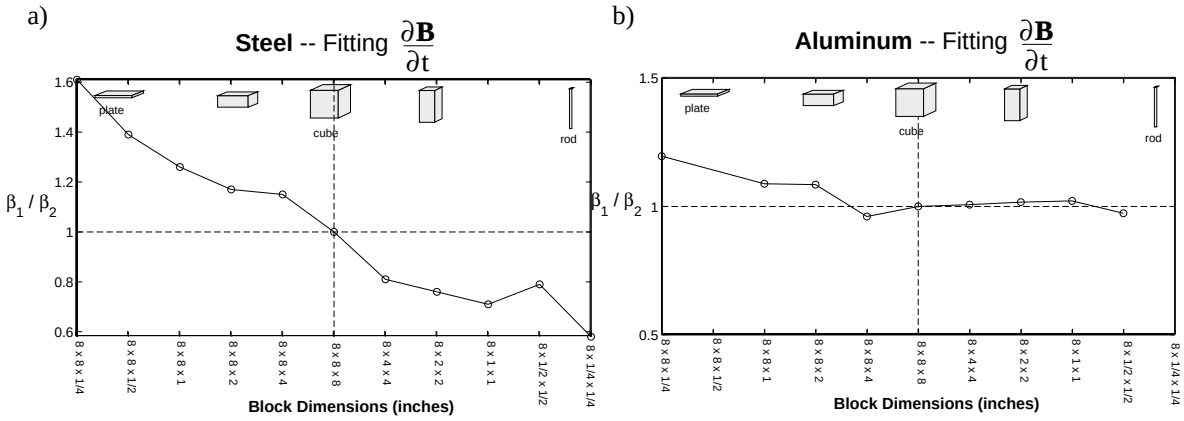

Figure 4: Relating the aspect ratio of a steel target with the ratio β_1/β_2. Plot (a) illustrates the relationship between the β_1/β_2 ratio derived from $\partial\mathbf{B}/\partial t$ data and the shape of a steel target. Plot (b) illustrates the relationship between the β_1/β_2 ratio and the shape of an aluminum target.

5 The Discrimination Algorithm Using $\partial\mathrm{B}/\partial t$ Data

The results from the previous section suggests the following algorithm for using $\partial\mathbf{B}/\partial t$ data to help identify possible UXO targets:

1. Perform the non-linear inversion recover model parameters for the two-dipole model.
2. Compute $\bar{\beta} = \frac{1}{2}(\beta_1 + \beta_2)$. If $\bar{\beta} > 0.80$ then the target is most likely permeable.
3. Compute ratios β_1/β_2 and k_1/k_2. There are two options:
   - $\bar{\beta} > 0.8 \Rightarrow$ *Ferrous Target*: If $k_1/k_2 > 1$ and $\beta_1/\beta_2 < 1$ then a permeable *rod-like* target was measured. If $k_1/k_2 < 1$ and $\beta_1/\beta_2 > 1$ then a permeable *plate-like* target was measured.
   - $\bar{\beta} < 0.8 \Rightarrow$ *Non-Ferrous Target*: If $k_1/k_2 > 1$ then a non-permeable *plate-like* target was measured. If $k_1/k_2 < 1$ then the target is *rod-like*. β_1/β_2 does not give any supporting, or extra, information.

The above algorithm can be extended to the analysis of $\mathbf{B}$-field data simply by changing the β threshold to 0.3 (Pasion, 1999).

(a) Location and Orientation

	m_o	m_{rec}	Expected Parameters
Northing (m)	1.85	1.92	2.00
Easting (m)	1.96	2.03	2.00
Burial Depth (m)	0.32	0.27	0.15
ϕ (degrees)	45	14.5	~ 0
θ (degrees)	45	51.7	~ 57

(b) Decay Parameters and Diagnostics

m_i	m_o	m_{rec}
k_1	7.82	10.89
α_1	0.020	0.014
β_1	1.09	0.94
γ_1	3.67	3.24
k_2	7.82	2.84
α_2	0.020	0.018
β_2	1.09	1.29
γ_2	3.67	2.96

Diagnostic	Result	Conclusion
$\bar{\beta}$	1.11	Permeable
k_1/k_2	3.84	Rod-like
β_1/β_2	0.73	Rod-like

Table 1: Recovered parameters for the field data inversion. Table (a) demonstrates that the inversion was successful in obtaining the approximate location and orientation of the target. Table (b) lists the recovered decay parameters of the two dipoles. Application of the diagnostics indicates that the buried target is permeable and rod-like and therefore a candidate for UXO.

6 Field Data Examples

6.1 Example 1: Small Survey over a Single Target

We apply our algorithm to a TEM field data set acquired at the United States Army Corps of Engineer Environmental Research and Development Center UXO test site in Vicksburg, Mississippi. The Geonics EM63 instrument was used for this survey. A 60 mm projectile was placed in the ground with its center at 2.0 m East, 2.0 m North and at a depth of 0.15 m from the surface. The projectile was placed at a dip of $\theta = 57$ °, with its tip pointing to the North ($\phi = 0$ °). The survey consisted of a $2m \times 2m$ grid centered on the target, containing 5 lines running North-South separated at $50cm$ line spacing, with stations located at $10cm$ intervals along each line.

The observed and predicted data are compared in figure 5. Fig. 5(a) shows a plan view comparison for four of the 26 time channels. Fig. 5(b) compares the observed and predicted data along three of the lines. Fig. 5(c) compares the decay curve measured at four stations on the survey.

The recovered location and orientation parameters are listed in Table 1(a). The recovered easting of $2.04m$ differs from the true value of $2.00m$ by $4cm$. The recovered northing of $1.77m$ differs from the true value of $1.83cm$ by $6cm$. These errors are of the same magnitude as can be expected in spotting the station location in the field survey. The recovered burial depth of $0.27m$ is $12cm$ deeper than the expected depth of $0.15cm$. This may be due to the instrument not responding strongly to the tapered aluminum tail of the 60 mm mortar. The orientation parameters θ and ϕ are well recovered. The recovered decay parameters are listed in Table 1(b) and the diagnostics applied to these parameters are listed in Table 1(c). The value of $\bar{\beta} = 1.11 (> 0.8)$ indicates that the target is likely magnetically permeable. The ratios $k_1/k_2 = 3.84 (> 1)$ and $\beta_1/\beta_2 = 0.73 (< 1)$ indicate, for a magnetically permeable target, that the TEM response is likely from a rod-like target.

6.2 Example 2: Data Extracted from a Large Scale Data Set

For this example we use data collected in a Geonics EM63 survey over the Ordnance Detection and Discrimination Study (ODDS) UXO seeded test plots at the former Fort Ord in California. A newly modified Geonics EM63 instrument was used for this survey. The survey consisted of $180ft$ long lines running East-West separated by $1ft$, with stations located at $10cm$ intervals along each line.

To remove the effects of instrument drift a 101 point median filter was used to calculate the long-wavelength trend along each acquisition line and for each channel. This trend line was removed from each channel. To create the image shown in fig. 6, time channels 2 to 10 were then averaged and a dc-shift applied to each line so that the median value of each line was constant across the survey. A bi-cubic spline gridding algorithm was then used to grid the data to a 0.25 ft pixel.

The inversion algorithm was applied to target 570 in the seeded plot, which is a 90 mm projectile located at $75.42ft$ East, $66.12ft$ North and at a depth of 30 inches from the surface. The projectile was placed in the ground horizontally ($\theta = 90$ °), with its tip pointing East ($\phi = 0$ °). An $8ft \times 8ft$ portion of the data was extracted about target 570 and inverted.

The observed and predicted data are compared in figure 7. Fig. 7(a) shows a plan view comparison for four of the 26

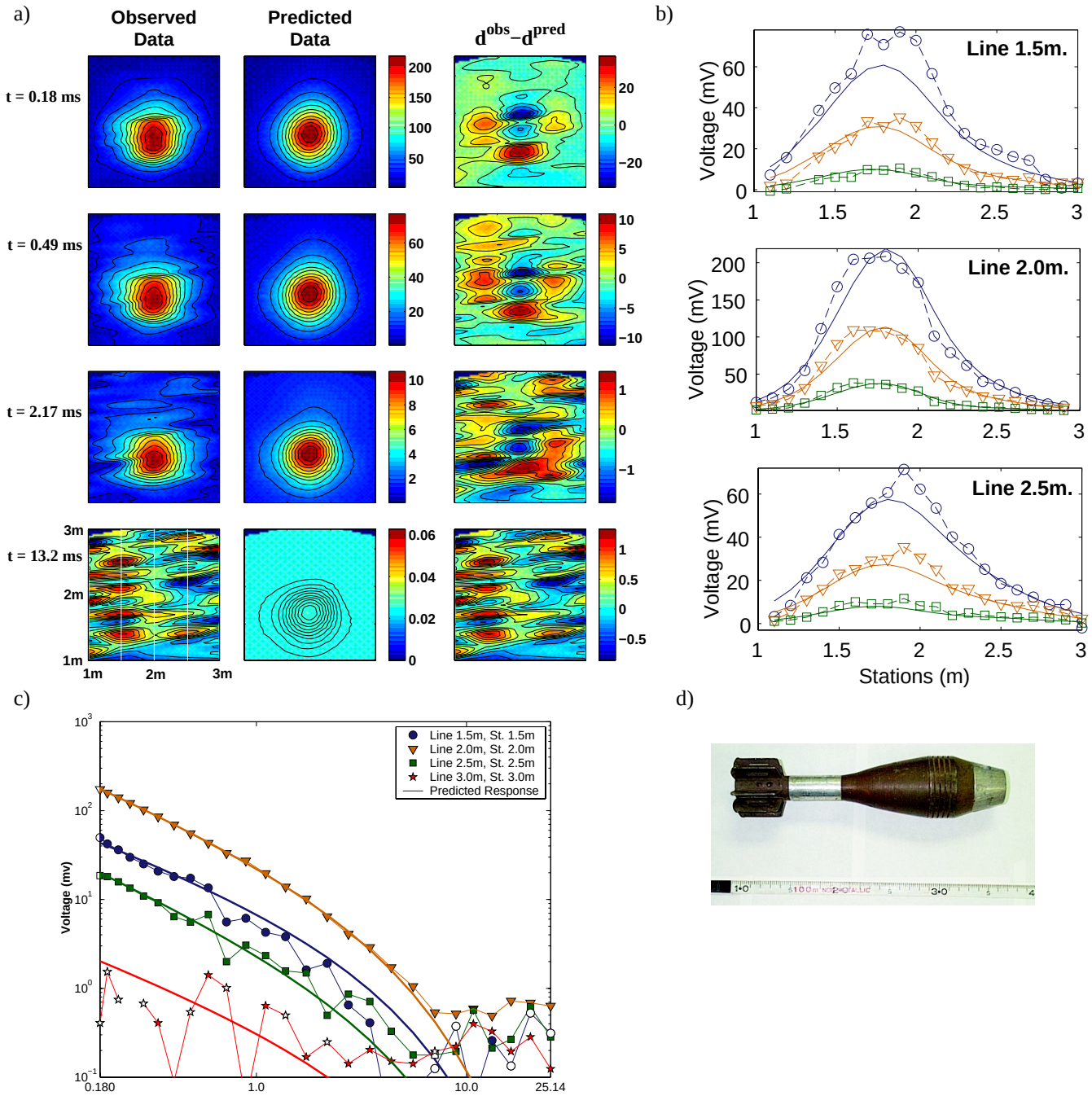

Figure 5: Plots of the observed and predicted data for the 60 mm projectile UXO field data set. (a) Plan view of the survey data for four of the time channels. It is clear that at t=13.2ms that the signal has fallen beneath the noise level of the instrument. The white lines in that plot indicate the lines of data used in the inversion. (b) Comparison of observed and predicted data along lines for times 0.18, 0.34, and 8.9ms. (c) Comparison of observed and predicted decay soundings at 4 stations. Symbols that are uncoloured (white) indicate that the absolute value has been plotted. (d) Photo of 60 mm projectile used in this survey.

time channels. Fig. 7(b) compares the observed and predicted data along three of the lines. Fig. 7(c) compares the decay curve measured at four stations on the survey. There are several possible reasons why the data appears noisier than in the previous data set: (1) The target is buried deeper and therefore has a weaker signal, (2) The lines were 180ft long, making accurate sensor positioning more difficult, and (3) The walking speed along each line of approximately 3ft/s was greater than in the first example.

(a) Location and Orientation

	m_o	m_{rec}	Expected Parameters
Easting (ft)	76.13	75.49	75.42
Northing (ft)	66.11	66.02	66.12
Burial Depth ($inches$)	24	23	30
ϕ (degrees)	45	5.5	~ 0
θ (degrees)	45	92.0	~ 90

(b) Decay Parameters and Diagnostics

m_i	m_o	m_{rec}
k_1	4.89	15.26
α_1	0.020	0.020
β_1	1.24	0.83
γ_1	23.21	21.02
k_2	4.89	4.42
α_2	0.020	0.020
β_2	1.24	1.02
γ_2	23.21	20.63

Diagnostic	Result	Conclusion
$\bar{\beta}$	0.92	Permeable
k_1/k_2	3.46	Rod-like
β_1/β_2	0.81	Rod-like

Table 2: Recovered parameters for the field data inversion. Table (a) demonstrates that the inversion was successful in obtaining the approximate location and orientation of the target. Table (b) lists the recovered decay parameters of the two dipoles. Application of the diagnostics indicates that the buried target is permeable and rod-like and therefore a candidate for UXO.

The recovered location and orientation parameters are listed in Table 2(a). The recovered easting of $75.49ft$ differs from the true value of $75.42ft$ by 0.84 inches. The recovered northing of $66.02ft$ differs from the true value of $66.12ft$ by 1.2 inches. These errors are of the same magnitude as can be expected in spotting the station location in the field survey. The recovered burial depth of $0.47m$ is $3cm$ deeper than the expected depths of $0.44m$. The orientation parameters θ and ϕ are well recovered. The recovered decay parameters are listed in Table 2(b) and the diagnostics applied to these parameters are listed in Table 2(c). The value of $\bar{\beta} = 0.92 (> 0.8)$ indicates that the target is likely magnetically permeable. The ratios $k_1/k_2 = 3.46 (> 1)$ and $\beta_1/\beta_2 = 0.81 (< 1)$ indicate, for a magnetically permeable target, that the TEM response is likely from a rod-like target.

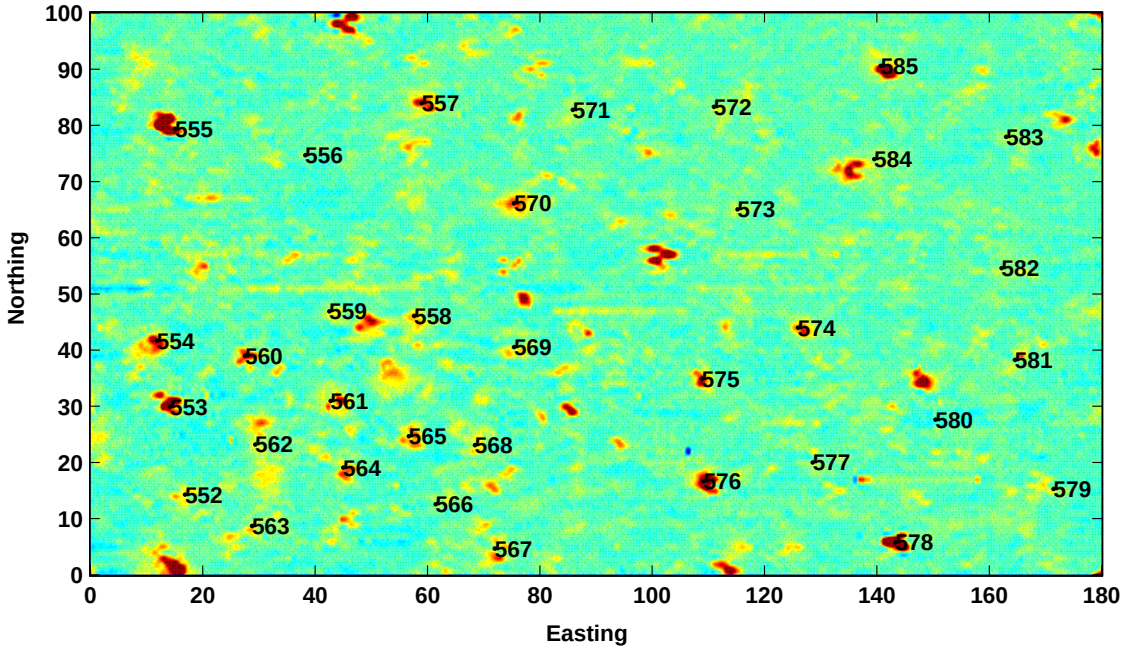

Figure 6: EM63 Survey Data collected over the ODDS Known 2 seeded test site at the former Fort Ord in California. This image was produced by removing a trend line from each time channel, then averaging channels 2 to 10. A dc-shift was applied to level the lines, and a bi-cubic spline gridding algorithm was used to create the image. Inversion algorithm is applied to data about target 570.

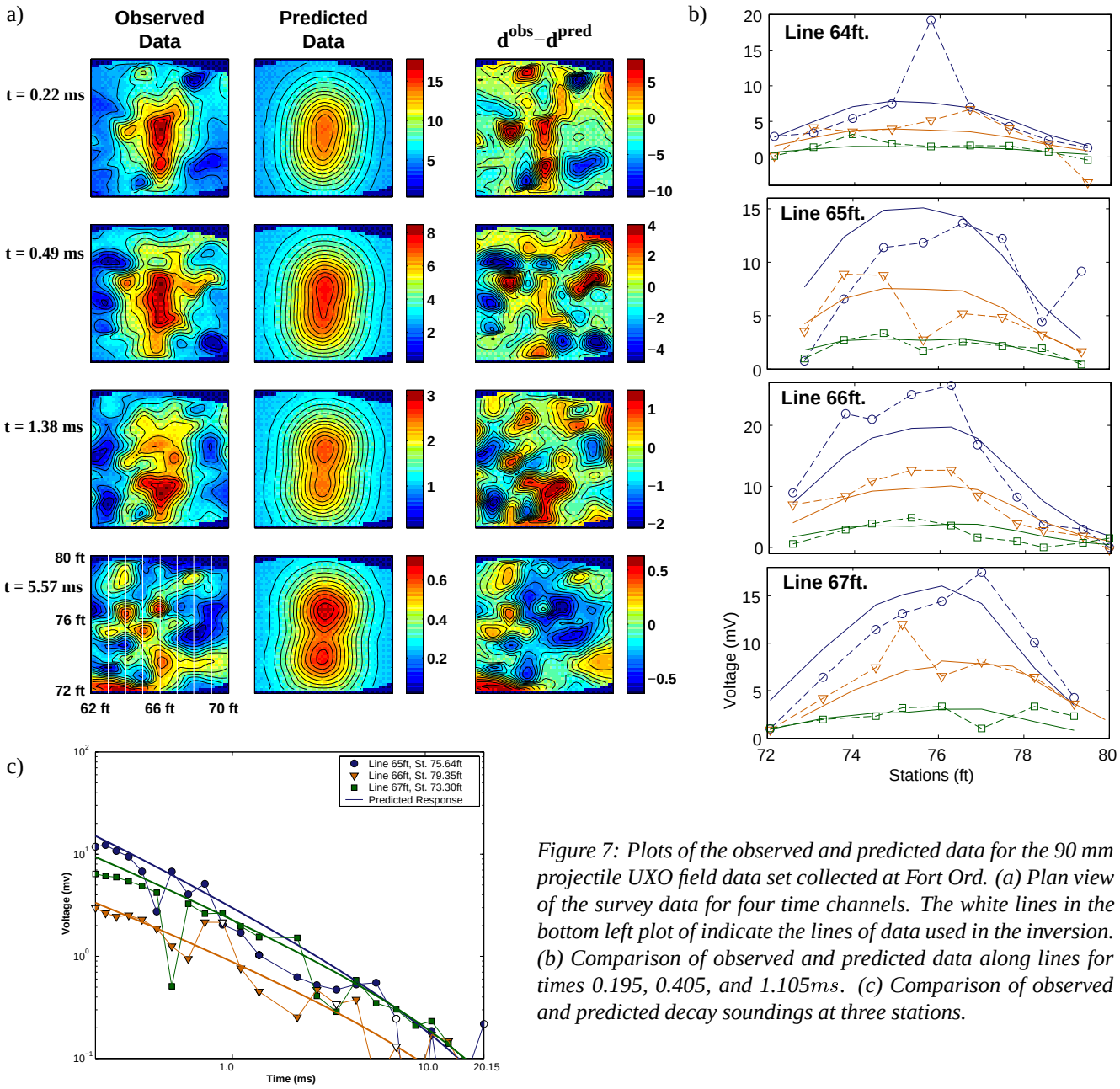

Figure 7: Plots of the observed and predicted data for the 90 mm projectile UXO field data set collected at Fort Ord. (a) Plan view of the survey data for four time channels. The white lines in the bottom left plot of indicate the lines of data used in the inversion. (b) Comparison of observed and predicted data along lines for times 0.195, 0.405, and 1.105ms. (c) Comparison of observed and predicted decay soundings at three stations.

7 Discussion and Conclusion

The TEM data inversion algorithm in Pasion and Oldenburg (2000) was applied to two field data sets. In both cases the diagnostics, applied to the recovered model parameters, correctly predicted that the TEM anomaly was produced by a magnetically permeable and rod-like metallic target. This supports the methodology proposed by Pasion and Oldenburg (2000). We recognize that further evaluations will be required and that an important ingredient to successful application to UXO discrimination will depend upon high quality data being recorded and state-of-the-art preprocessing applied to the data to extract the anomalous signal to be inverted. With such advances, the discrimination algorithm presented here has the potential for making a positive impact on the interpretation of UXO detection data.

8 Acknowledgments

We would like to thank the Presidio of Monterey, Directorate of Environmental and Natural Resources, and the US Army Corps of Engineers, Sacramento District. We also thank Jose Llopis and Mike Cormier at the US Army Corps of Engineers for help in acquiring EM63 data at the Fort Ord UXO test site. This work is supported in part by the U.S. Army Engineer Research and Development Center and the Army Research Office.

9 References

Carin, L., 2000, FEM Modelling of the EMI Response of General UXO Targets: Proceedings of UXO/Countermine Forum 2000.

Haber, E. and U.M. Ascher, 2000, Fast Finite Modelling of 3D Electromagnetic Problems With Highly Discontinuous Coefficients: SIAM Journal on Scientific Computing, accepted.

Hiptmair, R., 1998, Multigrid Method For Maxwell's Equations: SIAM Journal of Numerical Analysis, **36**, 204-225.

Kaufman, A.A., 1994, Geophysical Field Theory and Method: Academic Press, Inc.

Pasion, L.R., 1999, Detecting Unexploded Ordnance with Time Domain Electromagnetic Induction, M.Sc. Thesis, University of British Columbia.

Pasion, L.R., and D.W. Oldenburg, 2001, Locating and Determining Dimensionality of UXO Using Time Domain Electromagnetic Induction: Journal of Environmental and Engineering Geophysics, submitted.